Results in Engineering 30 (2026) 110076

Contents lists available at ScienceDirect

Results in Engineering

journal homepage: www.sciencedirect.com/journal/results-in-engineering

Research paper

Decarbonisation of lime kilns in ironmaking plants through Power to Gas

Manuel Bailera *, Alexander García-Mariaca, Cristian Barón

Energy and CO_2 Group, Aragon Institute of Engineering Research (I3A), Department of Mechanical Engineering, Escuela de Ingeniería y Arquitectura, Universidad de Zaragoza, María de Luna 3, 50018 Zaragoza, Spain

ARTICLE INFO

Keywords:
Power-to-Gas
Ironmaking
calcination
Methanation
Synthetic natural gas

ABSTRACT

The iron and steel industry is one of the world's major carbon emitters. Various decarbonisation options are currently being explored: Asian producers mainly focus on carbon capture and carbon recycling in blast furnaces, while European producers favour the use of hydrogen in direct reduction processes. While the latter can eliminate CO_2 emissions from iron ore reduction, producers still face CO_2 emissions in other plant processes. Lime kilns, which are essential to iron production, cannot be fully decarbonized through hydrogen or direct electrification alone, as CO_2 is inherently released during the calcination of limestone. Consequently, this paper analyses different decarbonisation pathways for lime kilns in ironmaking plants. These pathways utilize Power to Gas to establish carbon recycling concepts to avoid CO_2 emissions. The integration of Power to Gas was modelled and simulated for the following lime kiln technologies: (1) Parallel flow regenerative shaft air-fuel lime kiln with amine scrubbing, (2) Parallel flow regenerative shaft oxy-fuel lime kiln, and (3) Parallel flow regenerative shaft oxy-fuel H_2 lime kiln. The Power to Gas technology is powered by solar power. The PV solar field was modelled as being installed on the rooftops of a steelworks located in Austria. The total PV capacity that can currently be installed is 15 MWp. When considering additional roofs that require moderate rehabilitation or cleaning, the total PV capacity increases to 57 MWp. The results show that CO_2 emissions can be reduced by 2% to 28% compared to the conventional air-blown lime kiln case. However, CO_2 avoidance costs exceed 1,000 €/t_{CO2}, rendering the concept economically unfeasible.

1. Introduction: CO_2 emissions in iron and steel plants when shifting from coal to H_2

A conventional ironmaking plant has numerous CO_2 sources (Fig. 1), which arise from the use of coal, natural gas and limestone as raw materials. Limestone is calcined to obtain lime, which produces CO_2 (Eq. (1)). Lime has various uses within the steel industry as: (1) a binder in sinter production, (2) a desulfurizing agent, (3) a slag forming component for removing impurities, and (4) a component to control melt chemistry and reduce damage to furnace linings. The heat for calcination is supplied by the combustion of fossil fuels, such as natural gas, which leads to additional CO_2 emissions (Eq. (2)). The CO_2 content in the flue gas of a lime kiln is around 20vol% [1] (Table 1).

$$CaCO_3 \leftrightarrow CaO + CO_2 \quad (1)$$

$$CH_4 + 2O_2 \rightarrow CO_2 + 2H_2O \quad (2)$$

Coke is used in the sintering process, within coke ovens, and as an auxiliary fuel in blast furnaces. In sintering, coke is burned to agglomerate iron ore fines with other fine materials (under 10 mm in size) to produce an open-grained, consistent material with a definite basicity, which is optimal for the blast furnace burden. In addition, sintering allows for the recycling of dust and ferriferous materials by fusing them at high temperatures with iron ore fines, with little change to their chemical properties. The coke burned in the sinter strand produces CO_2 (Eq. (3)), which is emitted within the process flue gas. The CO_2 content of the sinter strand flue gas is around 8vol% [8].

$$CH_{2a}O_{2b}N_{2c}Z_z + d\ O_2 \rightarrow \alpha\ CO_2 + \beta\ CO + \gamma\ H_2O + \delta\ N_2 + \varepsilon\ Z \quad (3)$$

In the coke oven, coal is heated to 1100 °C in an oxygen-free atmosphere (a carbonization process) to drive off volatile matter and produce coke, which is a solid residue consisting primarily of carbon (Eq. (4)). The CO_2 content of the process flue gas is low, at about 2vol% [9]. However, since coke oven gas is used as a fuel in various other parts of the ironmaking plant, its subsequent combustion results in significant CO_2 emissions.

$$CH_{2a}O_{2b}N_{2c}Z_z \rightarrow \alpha\ CH_4 + \beta\ H_2 + \gamma\ CO_2 + \delta\ CO + \varepsilon\ N_2 + \epsilon\ C + \theta\ Z \quad (4)$$

Coke is the most critical raw material in the blast furnace. It acts as

* Corresponding author.
E-mail address: mbailera@unizar.es (M. Bailera).

https://doi.org/10.1016/j.rineng.2026.110076
Received 5 February 2026; Received in revised form 26 February 2026; Accepted 12 March 2026
Available online 15 March 2026

Nomenclature

Acronyms

BFG	Blast furnace gas
BOFG	Basic oxygen furnace gas
CO_2-eq	CO_2 equivalent emissions
COG	Coke oven gas
CSP	Concentrated solar power
I&S	Iron and steel
LDC	Load duration curve
LHV	Lower heating value
PCI	Pulverized coal injection
PFR	Parallel flow regenerative (shaft kiln)
PtG	Power to gas
PV	Photovoltaic
PVGIS	Photovoltaic geographical information system
SNG	Synthetic natural gas
THM	Ton of hot metal

Symbols

t	Operating hours, h
V	Volume produced/consumed/available, Nm^3
W	Electricity, kWh
w	Specific electricity consumption, kWh/Nm^3
$\dot{W}$	Power, kW

Greek symbols

δ	calculation parameter, h
ϵ	conversion efficiency, Nm^3_{SNG}/Nm^3_{H2}
η	efficiency, -
ν	stoichiometry of methanation, $mol_{H2}/(mol_{CO2}+mol_{CO})$
τ	storage capacity in terms of nominal operating hours, h

Subscripts and superscripts

$*$	Nominal load / full capacity
$\#$	Partial load
-	Dropped / discarded
1	Interval of 1-hour duration
b	Li-ion battery
e	Electrolyser
i	Lime kiln configuration i
j	Hour j of the year
m	methanation
p	Peak power
PV	Photovoltaic panels
s	H_2 storage / H_2 tank

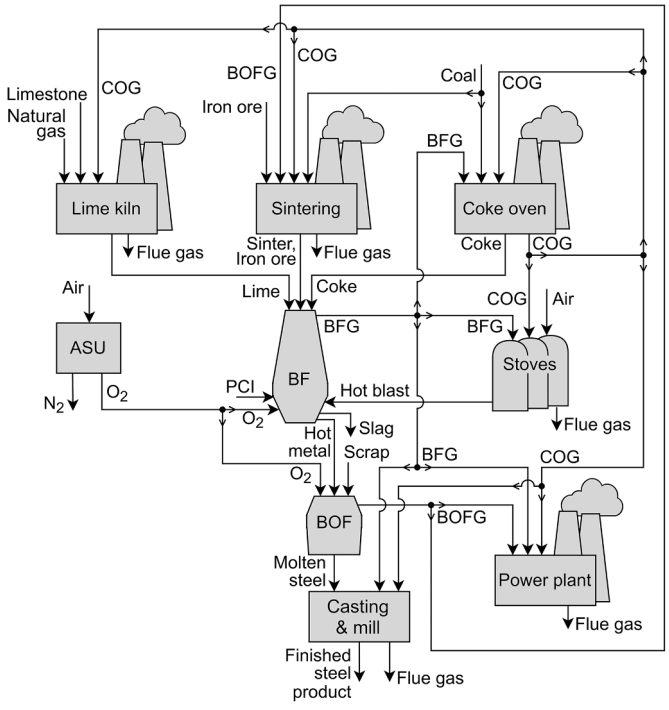

Fig. 1. Example of a process flow diagram of an integrated I&S plant (not all plants have the same configuration).

reducing agent to reduce iron ore directly (Eq. (5)) and indirectly (via the CO obtained from coke combustion, Eqs. (6) to (8)). Coke also provides mechanical stability and permeability inside the furnace, ensuring the ascent of the reducing gases, as well as optimal resource utilization and high productivity. Pulverized coal injection can be used as an auxiliary fuel in the lower part of the furnace to decrease coke consumption. The top gas produced in the blast furnace mainly consists of CO_2 from the reduction reactions, unreacted CO, and N_2 from the blast air. The CO_2 content is around 23vol%. Similar to coke oven gas, this blast furnace gas can be used as a fuel in other plant processes, which results in further CO_2 emissions. One of the main users of blast furnace gas is the hot blast stoves, which use this fuel gas to preheat the air entering the blast furnace.

Table 1
Typical composition (vol%) of flue gases in an I&S plant [2–7].

Flue gas from	CO_2	CO	H_2O	H_2	CH_4	C_2H_4	N_2	O_2
Lime kiln	15 – 25	-	5 – 15	-	-	-	50 – 70	1 – 9
Sintering	1 – 8	0 – 1	2 – 10	-	-	-	66 – 77	15 – 20
Coke oven	1 – 3	4 – 8	0 – 4	39 – 65	20 – 42	0 – 2	2 – 8	0 – 1
Blast furnace	17 – 25	20 – 28	2 - 3	1 – 5	-	-	46 – 55	-
Stoves	20 – 30	-	5 – 15	-	-	-	52 – 69	0 – 1
BOF	14 – 16	57 – 73	0 – 12	0 – 3	-	-	8 – 14	-
Casting & mill	10 – 30	0 – 2	5 – 20	-	-	-	50 – 90	0 – 5
Power plant	15 – 20	-	5 – 15	-	-	-	50 – 80	0 – 7

$$FeO + C \rightarrow Fe + CO \quad (5)$$

$$3Fe_2O_3 + CO \rightarrow 2Fe_3O_4 + CO_2 \quad (6)$$

$$Fe_3O_4 + CO \rightarrow 3FeO + CO_2 \quad (7)$$

$$FeO + CO \rightarrow Fe + CO_2 \quad (8)$$

Another process that emits CO_2 is the basic oxygen furnace. Here, the

carbon content of the hot metal is diminished by oxidation to obtain steel (Eq. (9)). Part of the CO produced in the process is also oxidised to CO_2 because of the presence of oxygen (Eq. (10)). The CO_2 content of the BOF gas is around 16vol%. The carbon that is dissolved in the hot metal came from the coke used in the blast furnace, which in turn came from the coal used in the coke oven.

$$C + \frac{1}{2}O_2 \rightarrow CO \quad (9)$$

$$CO + \frac{1}{2}O_2 \rightarrow CO_2 \quad (10)$$

During the casting of the steel, mainly coke-oven gas and some blast-furnace gas are used for reheating purposes. The exhaust gas has a low CO_2 content (7vol%) due to the high H_2 content of the coke oven gas [10]. The remaining fuel gases are used to generate electricity in a power plant. The most common technology is combined cycle, whose exhaust gas typically contains 17% CO_2 for this type of fuel gases.

Attending to all the CO_2-emitting processes of iron and steel plants, one realises that coal is behind most of them, driven by the necessity of coke in the blast furnace. In the near future, this scenario may drastically change with the adoption of new technologies based on the direct reduction of iron ore by H_2 (Eqs. (11) to (13)). Direct reduction refers to solid-state processes that reduce iron ore to metallic iron at temperatures below the melting point (below 1200 °C). The iron obtained this way is called direct reduced iron (DRI) or sponge iron [11]. If the direct-reduced iron is compacted at densities above 5,000 kg/m^3, it is considered a premium form of DRI and called hot briquetted iron (HBI).

$$3Fe_2O_3 + H_2 \rightarrow 2Fe_3O_4 + H_2O \quad (11)$$

$$Fe_3O_4 + H_2 \rightarrow 3FeO + H_2O \quad (12)$$

$$FeO + H_2 \rightarrow Fe + H_2O \quad (13)$$

The utilisation of shaft furnaces for DRI, instead of blast furnaces, will avoid the emissions of the latter, but also the emissions of coke making, which will no longer be needed. At the same time, those processes using blast furnace gas and coke oven gas will shift to H_2 to fulfil their heat requirements. In addition, the power plant might disappear if there are no fuel gases to take advantage of, thus being replaced by direct renewable electricity (wind or solar power). In the case of sintering, the palletisation of iron ore will still be required for DRI, for which some solid fuel will have to be consumed. Recently, Vale (mining company) produced iron ore pellets using plant-based biochar for the first time, instead of anthracite coal [12]. Moreover, other biomass fuels have been studied from a theoretical point of view by Sefidari et al [13], who concluded that pyrolysis oils could be the most viable alternative to coal in the pelletizing processes. Therefore, it is very likely that pelletizing will switch to CO_2-neutral fuels in the future as well. On its part, the basic oxygen furnace will be replaced by an electric arc furnace (EAF) to achieve the required steel grade through carburization [14]. In the EAF, DRI and/or HBI are charged together with alloying elements, slag formers (such as lime) and carbon sources to control the carbon content of the melt. As for pelletisation, some authors already studied the possibility of using biomass or biochar as carbon sources for the EAF process [15]. Therefore, any CO and CO_2 in the exhaust gas of the EAF will come from CO_2-neutral fuels. Lastly, the lime kiln, which is necessary for slag control, may run on renewable fuels to provide the heat for calcination. However, calcination of limestone will always produce CO_2 that does not come from CO_2-neutral fuels. Still, from the limestone itself (Eq. (1)). Thus, when in the near future steel producers shift from coal to H_2, they will be able to avoid all CO_2 emissions except for those coming from lime production.

The objective of the present paper is to propose and analyse four different pathways for decarbonising lime kilns in ironmaking plants. These concepts are based on methanation, which produces synthetic methane by combining CO_2 with renewable H_2 (Eq. (14)).

$$CO_2 + 4\ H_2 \rightarrow CH_4 + 2\ H_2O \quad (14)$$

The novelty of the present papers lies in the fact that none of the proposed concepts has been analysed before in the context of a future H_2-based steelmaking industry, where the only remaining emissions are those from lime kilns. Moreover, some of the proposed concepts are entirely new and can be extrapolated to other industries (e.g., cement industry). All the proposed solutions are based on commercially available or under-research technologies in industrial pilot plants. In addition, the required renewable electricity is assumed to come from photovoltaic panels installed in the different buildings of an ironmaking plant located in Austria, by quantifying the available roof with Google Earth. The paper is completed with the techno-economic analysis of the proposed solutions. The study comprises: (1) the description of the decarbonisation technologies proposed, (2) the methodology on both the PV solar field and the methanation plant sizing and management, (3) the methodology for simulating the different decarbonisation technologies, (4) the methodology on techno-economic analysis, (5) the assessment on the renewable electricity and H_2 production under two different scenarios, (6) the assessment on CO_2 emissions reduction, and (7) the analysis of cash flow, pay-back and internal rate of return of the concepts.

2. Decarbonisation pathways based on Power to Gas for lime kilns

Calcination is a chemical reaction that dissociates limestone ($CaCO_3$) into lime (CaO) and CO_2 by consuming thermal energy at high temperature (>850 °C). This CO_2 must be consumed, recycled or stored to avoid its release into the atmosphere. In our study, we opted for methanation (Eq. (14)) since hydrogen will be produced in large

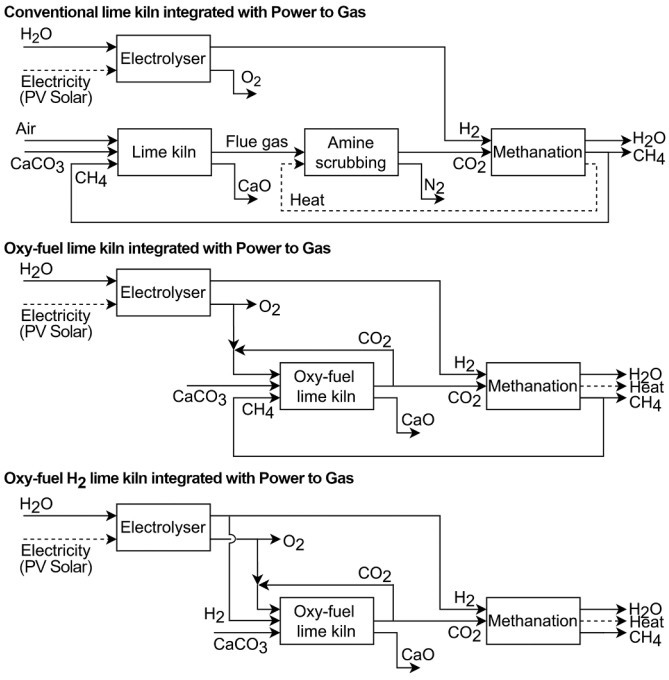

Fig. 2. Decarbonisation options based on Power to Gas for lime kilns.

quantities in a future H_2-based DRI steelmaker. Additionally, the thermal energy required for calcination should be provided by CO_2-neutral synthetic fuels, hydrogen or even concentrated solar power, to avoid further emissions. Considering these premises, three decarbonisation options were analysed. These are presented in Fig. 2, considering that all fossil natural gas is replaced and that all CO_2 is sent to methanation. In practice, reliance on some fossil fuels and/or the inability to fully utilise CO_2 may persist if renewable electricity proves insufficient. Additionally, hydrogen availability may remain limited in the medium term.

- Conventional lime kiln integrated with amine scrubbing and Power to Gas: The first decarbonisation option combines air-blown lime kilns (conventional technology) with amine scrubbing to capture the CO_2 emissions. Then, the captured CO_2 is sent to the methanation stage, where it is combined with renewable hydrogen and produce synthetic methane. Part of this synthetic methane is used in the lime kiln to replace the fossil natural gas. In addition, the amine scrubbing takes advantage of the exothermic heat from methanation to provide heat to the reboiler of the CO_2 desorption tower.
- Oxy-fuel lime kiln integrated with Power to Gas: The second decarbonisation option is an oxy-fuel lime kiln. This uses a mixture of pure O_2 and recirculated flue gas as an oxidising agent in combustion, instead of air. The recirculated CO_2 replaces the N_2 in the air to maintain operating conditions like those of conventional technologies. Thanks to the oxy-fuel conditions, CO_2 concentrations above 90vol% can be achieved in the exhaust gas, thus avoiding amine scrubbing [16]. Moreover, oxy-fuel lime kilns can take advantage of the O_2 produced during the water electrolysis stage. As in the previous decarbonisation option, CO_2 is used to produce synthetic methane, which replaces the fossil natural gas in the lime kiln.
- Oxy-fuel H_2 lime kiln integrated with Power to Gas: The third decarbonisation option is also an oxy-fuel lime kiln, like in the previous case, but now hydrogen is used as fuel. The CO_2 from calcination is used to perform methanation. Since this lime kiln does not consume natural gas, the synthetic methane is injected into the grid for sale.

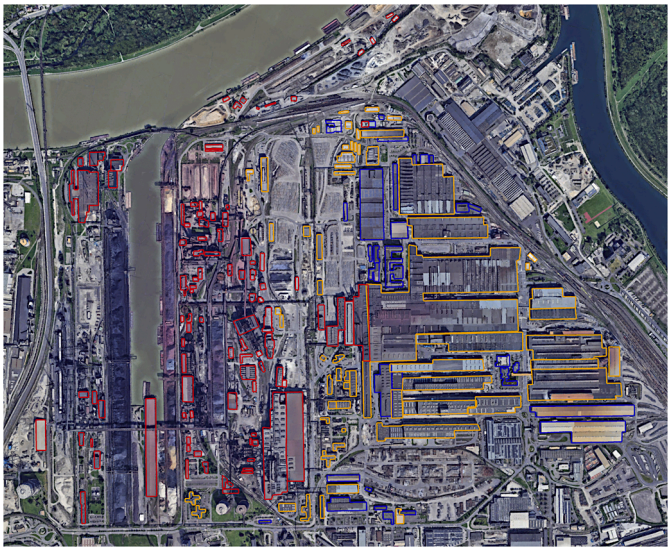

Fig. 3. Satellite image for a steelworks located in Austria (48°16′38.2"N, 14°19′58.7"E) [20]. Blue: Type 1 roof, Yellow: Type 2 roof, Red: Type 3 roof.

3. Methodology

3.1. Sizing and management of the PV solar field

The PV solar field was assumed to be installed on the roofs of the various buildings at a steelworks in Austria (Fig. 3). The available roof area was delimited in Google Earth and quantified in QGIS. The roofs were classified into three categories:

- Type 1: These roofs are assumed to be ready for PV panel installation, and their operation would not be notably affected by surrounding conditions (shadows, dust, etc.).
- Type 2: These roofs need conditioning to install PV panels and/or moderate measures to mitigate ambient dust from nearby processes. Hence, additional investment would be required.
- Type 3: These roofs require remarkable modifications and/or extreme measures against the ambient dust from nearby processes, hence jeopardising the economic viability of the PV panels.

The electricity production from the PV panels was calculated using the PVGIS tool from the European Commission (version 5.2) and the PVGIS-SARAH2 database [17]. The mounting type was assumed fixed, and the PVGIS tool optimised the panels' slope and azimuth. The PV technology was crystalline silicon, and the system loss was fixed at 20%, which is higher than the default value of 14% because of the expected ambient dust in the steelworks (it must be noted that this loss does not include losses related to the angle of incidence and temperature, which are already estimated and taken into account by the PVGIS tool according to the satellite data). The data on electricity production were retrieved hourly for 1 kWp of power capacity, at latitude 48.271 and longitude 14.336, for the year 2019 (Table 2). This electricity production was then scaled up to the total peak power that can be installed in the available solar area by assuming 15% efficiency [18,19] of the PV panels (Eq. (15)). The available solar area is assumed 70% for Type 1 roof, 50% for Type 2 roof, and 0% for Type 3 roof.

$$\text{Peak power}\ [\text{kWp}] = \text{Solar area}\ [\text{m}^2] \times \text{PV panel efficiency}\ [-] \quad (15)$$

Additionally, a Li-ion battery was included to mitigate variations in the electricity production from the PV panels, which might occur due to cloud coverage. The nominal power of the battery ($\dot{W}_b^*$) was assumed to be 5% of the total peak power of the PV solar field ($0.05\dot{W}_{PV,p}^*$) [21], the efficiency of the battery (η_b) was set at 85% [22,23], and its energy

Table 2
Location and technical data of the PV solar field.

Parameter	Data
Location	Linz, Austria
Latitude (dec)	48.271
Longitude (dec)	14.336
Type 1 roof	
N° buildings	30
Roof area (m^2)	141,048
Solar area (m^2)	98,734
Type 2 roof	
N° buildings	64
Roof area (m^2)	563,053
Solar area (m^2)	281,527
Type 3 roof	
N° buildings	101
Roof area (m^2)	221,130
Solar area (m^2)	0
PV technology	Crystalline silicon
PV system loss (%)	20
PV panel efficiency (%)	15
PV panel slope (°)	38
PV panel azimuth (°)	1

capacity equal to 4 h of nominal operation (τ_b) [21,22]. The electricity available in the Li-on battery at hour j ($W_{b,j}$) depends on the PV electricity production ($W_{PV,j-1}$) and the charge of the battery ($W_{b,j-1}$) at the preceding hour $j-1$, and on the electrolyser consumption at nominal load for 1 hour ($W^*_{e,1}$) (Eq. (16)).

$$W_{b,j} = \begin{cases} W^*_b & \text{if } W_{PV,j-1} \geq W^*_{e,1} \text{ and } \left(\left(W_{PV,j-1} - W^*_{e,1}\right)\eta_b + W_{b,j-1}\right) \geq W^*_b \\ \left(W_{PV,j-1} - W^*_{e,1}\right)\eta_b + W_{b,j-1} & \text{if } W_{PV,j-1} \geq W^*_{e,1} \text{ and } \left(\left(W_{PV,j-1} - W^*_{e,1}\right)\eta_b + W_{b,j-1}\right) < W^*_b \\ \left(W_{PV,j-1} + W_{b,j-1}\right) - W^*_{e,1} & \text{if } W_{PV,j-1} < W^*_{e,1} \text{ and } \left(W_{PV,j-1} + W_{b,j-1}\right) \geq W^*_{e,1} \\ 0 & \text{if } W_{PV,j-1} < W^*_{e,1} \text{ and } \left(W_{PV,j-1} + W_{b,j-1}\right) < W^*_{e,1} \end{cases} \quad (16)$$

It should be noted that the available electricity in the battery is accounted for after losses. At full capacity (W^*_b), it is equal to its nominal power capacity ($\dot{W}^*_b$) multiplied by the equivalent hours of energy storage (τ_b), accounting for losses (i.e., $W^*_b = \tau_b \eta_b \dot{W}^*_b$).

3.2. Sizing and management of the Power to Gas plant

Once both the electricity produced by the PV panels (data from PVGIS scaled by Eq. (15)) and the electricity provided by the Li-ion battery (Eq. (16)) were known, the electricity consumed by the electrolyser was computed through Eq. (17).

$$W_{e,j} = \begin{cases} W^*_{e,1} & \text{if } W_{PV,j} \geq W^*_{e,1} \\ W^*_{e,1} & \text{if } W_{PV,j} < W^*_{e,1} \text{ and } \left(W_{PV,j} + W_{b,j}\right) \geq W^*_{e,1} \\ W_{PV,j} + W_{b,j} & \text{if } \left(W_{PV,j} + W_{b,j}\right) < W^*_{e,1} \end{cases} \quad (17)$$

In order to select $W^*_{e,1}$ (which is the nominal electricity consumption of the electrolyser in 1 hour, $W^*_{e,1} = 1 \cdot W^*_e$), the electrolyser was sized using the load duration curve (LDC) (Fig. 4). This curve relates the nominal operating load of the electrolyser ($\dot{W}^*_e$) with the maximum operating hours that it might work at that load ($t_{\dot{W}^*_e}$, Eq. (18)).

$$t_{\dot{W}^*_e} = \sum_j \delta_j \quad \text{where} \quad \delta_j = \begin{cases} 0 & \text{if } W_{e,j} < W^*_{e,1} \\ 1 & \text{if } W_{e,j} = W^*_{e,1} \end{cases} \quad (18)$$

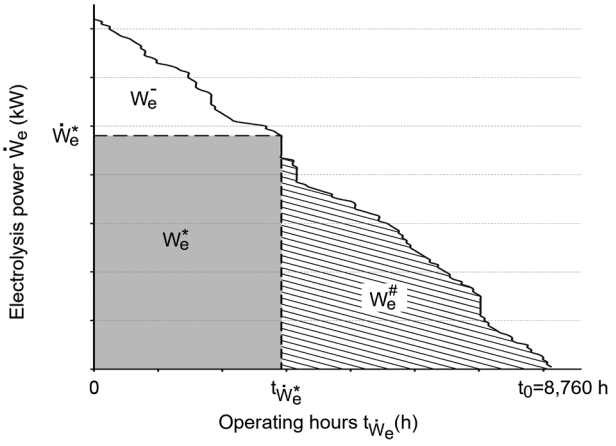

Fig. 4. Load duration curve methodology (blank area: energy discarded; grey area: energy processed at nominal load; pattern area: energy processed at partial load).

The product of the two values ($\dot{W}^*_e \cdot t_{\dot{W}^*_e}$) is a measure of the electrical energy that could be processed by the electrolyser at nominal load (W^*_e). The main criterion (criterion 1) for selecting the nominal power capacity of the electrolyser was to maximise the energy processed at nominal load (i.e., maximisation of W^*_e, the grey area under the LDC, in Fig. 4) [24]. In some cases, large variations in the resulting nominal load (e.g., $\dot{W}^*_e \pm 15\%$) only produced small changes in the energy processed at nominal load ($W^*_e \pm 0.1\%$), but the total energy processed remarkably changed ($(W^*_e + W^\#_e) \pm 6\%$). Hence, in these cases, a second criterion (criterion 2) was added to avoid ambiguity: the nominal load derived from the maximisation process was increased by progressively decreasing W^*_e at -0.25% intervals until the relative increment in the total processed energy dropped below 1%. Graphically, this means that the grey area (W^*_e) was diminished at -0.25% intervals by increasing $\dot{W}^*_e$ in Fig. 4, until the total area composed by $W^*_e + W^\#_e$ stopped increasing beyond 1% in a single step. This way, we had an electrolyser with a very similar operational optimisation (nearly the same amount of energy processed at nominal load), but with a notable greater total energy processed (i.e., the blank area of discarded energy W^-_e notably decreased, the pattern area of energy processed at partial load $W^\#_e$ increased in the same amount, and the grey area of energy processed at nominal load W^*_e barely changed).

The amount of H_2 produced by the electrolyser was calculated using Eq. (19), which is directly dependent on the electricity supplied. The specific consumption, w_e, was set at 4.5 kWh/Nm^3, corresponding to a commercial containerised PEM electrolyser in the M scale [25].

$$V_{H_2,e,j} = W_{e,j} / w_e \quad (19)$$

This H_2 was either sent to storage or to methanation, depending on the H_2 hourly production of the electrolyser ($V_{H_2,e,j}$) and on the nominal H_2 consumption of the methanation plant ($V^*_{H_2,m,1}$). The H_2 available in the tank at each hour was calculated using Eq. (20), and the H_2 consumption of the methanation plant was calculated using Eq. (21).

$$V_{H_2,s,j} = \begin{cases} V_{H_2,e,j-1} + V_{H_2,s,j-1} - V^*_{H_2,m,1} & \text{if } \left(V_{H_2,e,j-1} + V_{H_2,s,j-1}\right) > V^*_{H_2,m,1} \\ 0 & \text{if } \left(V_{H_2,e,j-1} + V_{H_2,s,j-1}\right) \leq V^*_{H_2,m,1} \end{cases} \quad (20)$$

$$V_{H_2,m,j} = \begin{cases} V^*_{H_2,m,1} & \text{if } \left(V_{H_2,e,j} + V_{H_2,s,j}\right) \geq V^*_{H_2,m,1} \\ V_{H_2,e,j} + V_{H_2,s,j} & \text{if } \left(V_{H_2,e,j} + V_{H_2,s,j}\right) < V^*_{H_2,m,1} \end{cases} \quad (21)$$

The Eq. (20) assumes no limit on the H_2 storage, so the required size for the H_2 tank is $\max_j\left(V_{H_2,s,j}\right)$. This value is entirely dependent on methanation plant size: the smaller the methanation plant, the larger the H_2 tank (unsuitable for technical and economic viability) and the higher the methanation plant's capacity factor (suitable for steady operation). Hence, we minimised the methanation plant size in order to increase its equivalent operating hours, subject to the constraint: $\max_j\left(V_{H_2,s,j}\right) \leq 66,740$ (constrained minimisation solver). This limit is intended for the storage of 6,000 kg of H_2 (i.e., 66,740 Nm^3), which corresponds to the H_2 storage installed in Puertollano (Spain) by Iberdrola at a 100 MW PV

solar plant aimed at producing of green H_2.

The H_2 is stored at 60 bar in 11 tanks, each 133 m^3 each (23.5 m in height, 2.8 m in diameter and 4.5 cm in thickness) [21]. The SNG production (Eq. (22)) and the CO_2-eq consumption (Eq. (23)) will depend on the lime kiln configuration selected, due to differences in flue gas composition.

$$V_{SNG,m,j} = \begin{cases} V^*_{H_2,m,1}\epsilon_{m,i} & if\ \left(V_{H_2,e,j} + V_{H_2,s,j}\right) > V^*_{H_2,m,1} \\ \left(V_{H_2,e,j} + V_{H_2,s,j}\right)\epsilon_{m,i} & if\ \left(V_{H_2,e,j} + V_{H_2,s,j}\right) \le V^*_{H_2,m,1} \end{cases} \quad (22)$$

$$V_{CO_2-eq,m,j} = \begin{cases} V^*_{H_2,m,1} \Big/ \nu_{m,i} & \text{if} \left(V_{H_2,e,j} + V_{H_2,s,j}\right) > V^*_{H_2,m,1} \\ \left(V_{H_2,e,j} + V_{H_2,s,j}\right) \Big/ \nu_{m,i} & \text{if} \left(V_{H_2,e,j} + V_{H_2,s,j}\right) \le V^*_{H_2,m,1} \end{cases} \quad (23)$$

The parameters $\epsilon_{m,i}$ (gas conversion efficiency) and $\nu_{m,i}$ (stoichiometry of methanation) were calculated in Aspen Plus for each configuration.

3.3. Modelling of the lime kiln and Power to Gas plants

3.3.1. Air-blown lime kiln with amine scrubbing

The first decarbonisation option combines an air-blown lime kiln and amine scrubbing. The calcination technology used in steelworks is normally a PFR kiln (parallel-flow regenerative shaft kiln). It consists of two vertical shafts and a connecting crossover channel (Fig. 5). Both shafts work together: one calcines the product and the other preheats the stone. In the burning shaft, the lime is calcined in parallel-flow system. The hot combustion gases are then transferred through the crossover channel to the non-burning shaft, where they preheat the limestone in a counterflow arrangement. The flow direction of the gases is reversed at regular intervals, alternating the function of the shafts [26].

The PFR kiln was modelled in Aspen Plus, assuming a typical lime production of 200 t/d. The burning shaft comprises a RGibbs reactor and a heat exchanger. The reactor limits the maximum $CaCO_3$ conversion to 98.5%, and considers Fe_2O_3, SiO_2 and Al_2O_3 as non-reacting components. The heat exchanger cools the lime with the air entering at the bottom, which is heated to 950 °C. The non-burning shaft accounts the heat transfer between the gases (exiting at 100 °C) and the limestone, during the preheating of the solids. The simulation used the PENG-ROB property method, based on the Standard Peng-Robinson cubic equation of state [27].

The amine scrubbing model was elaborated from an Example File provided by Aspen Plus for MDEA [28]. Before diverting the flue gas to the capture plant, water was condensed at 35 °C. The CO_2 capture ratio was fixed at 90%. The clean gas exits the absorber at 1 bar and 42 °C, while the CO_2-rich gas exits the amine plant at 1 bar and 35°C (after condensation) with a CO_2 content of 95.9vol%. The heat demand for the stripper reboiler is 3.6 MJ/kg_{CO2}, which can be supplied with the exothermic heat from methanation. A detailed description of the amine plant is available in [29].

3.3.2. Oxy-fuel lime kiln

The second decarbonisation option is an oxyfuel PFR kiln (Fig. 6). In this case, recirculation gas enriched with oxygen is used as an oxidising agent instead of air. In addition, the cooling air at the bottom is extracted from the kiln before it can mix with the combustion gas, thereby preventing N_2 from entering the flue gas. Recirculation gas is also used to recover the heat from the cooling air and then injected into the connecting channel (to replace the discharged cooling air), thus maintaining similar mass flow conditions. This technology, developed by Maerz, is known as the EcoKiln system [30]. This type of oxyfuel PFR kilns allows selecting both conventional air-blown operation and oxyfuel operation, providing greater flexibility in terms of economic efficiency. In the oxyfuel mode, CO_2 concentrations above 90vol% in the exhaust gas, and lime productions of up to 800 t/d can be achieved [16].

The Aspen Plus model of the oxyfuel PFR considered the burning shaft (RGibbs reactor and heat exchanger for cooling) and the non-burning shaft (heat exchanger for preheating solids), as in the previous case, and included the necessary additional equipment for gas recirculation. To moderate the combustion temperature, the O_2 was mixed with flue gas. The amount of gas recirculated was fixed to obtain the same lime temperature at the outlet of the RGibbs reactor as in the air-blown PFR kiln. Additionally, the cooling air was discharged before entering the calcination stage (to avoid N_2 presence in the exhaust gas) and replaced with an equivalent recirculated mass flow through the connecting channel. The cooling air, which reached 950 °C after cooling the lime, is used to preheat the second recirculation to 750 °C. A further heating of the recirculation to 920 °C was necessary to prevent recarbonisation of the already calcined product (this is usually performed using a small oxyfuel burner or an electric flow heater) [16]. The simulation used the PENG-ROB property method, based on the Standard Peng-Robinson cubic equation of state [31].

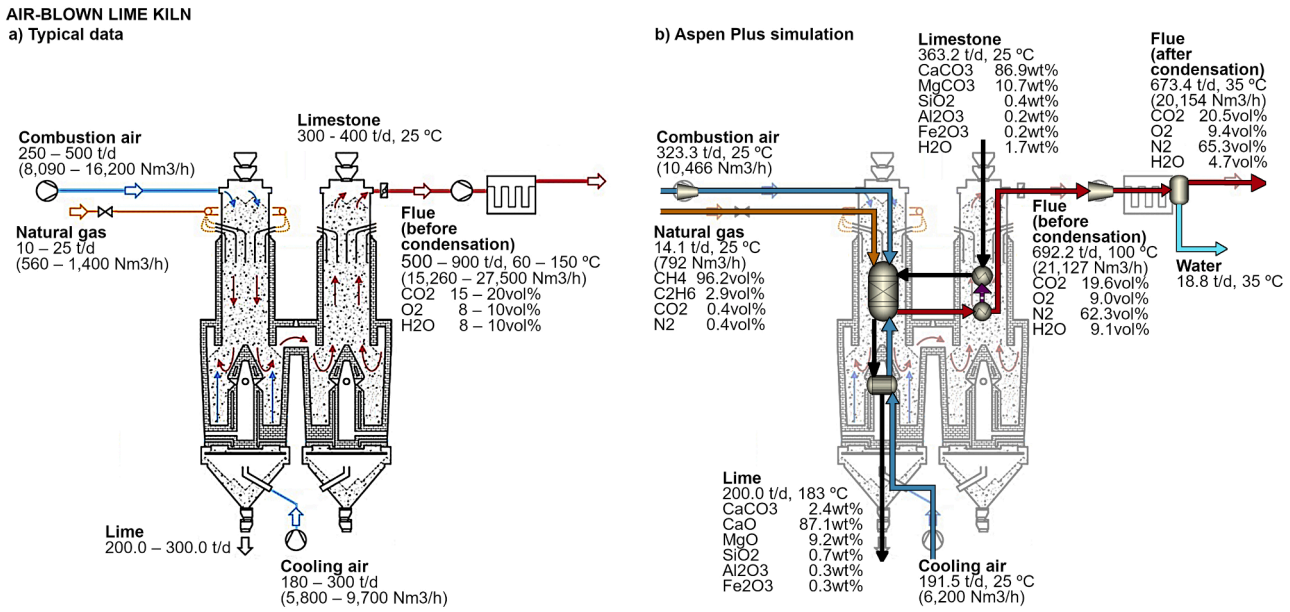

Fig. 5. Conceptual diagram (left) and Aspen Plus simulation (right) of an air-blown parallel flow regenerative lime kiln.

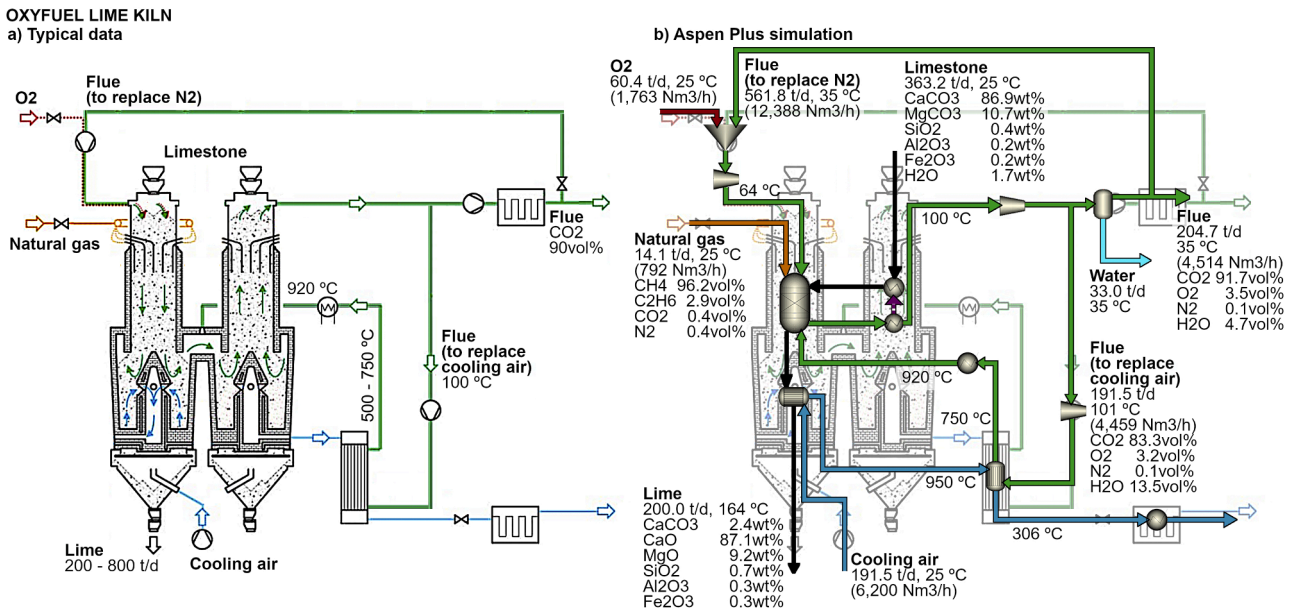

Fig. 6. Conceptual diagram (left) and Aspen Plus simulation (right) of an oxyfuel parallel flow regenerative lime kiln.

3.3.3. *Oxy-fuel H_2 lime kiln*

The third decarbonisation option is an oxyfuel PFR kiln, as in the previous case, but fuelled with H_2 instead of natural gas. The assumptions on temperatures and recirculation, as well as the property methods and models selected in Aspen Plus, are the same as in the previous case. The process flow diagram is presented in Fig. 7.

3.3.4. *Methanation plant*

The methanation plant is based on the technology developed by Hitachi Zosen Corporation. Their technology comprised two shell-and-tube typed exchange reactors, operating at 5 bar and 250 °C, with an intermediate condensation stage. The final CH_4 content of the synthetic natural gas was 98.5vol%, and the H_2 content was 1.3vol%, on a dry basis [32]. The corresponding Aspen Plus model consisted of two 2-stage compressors for the inlet CO_2 and H_2 (compression ratios of 2.5:1 and 2:1, with intermediate cooling at 60 °C), two RGibbs equilibrium reactors for the methanation stages (at 250 °C and 5 bar), two Flash reactors for water condensation after each methanator (at 50 °C and 35 °C), and two preheating exchangers before each methanator (at 250 °C). Additionally, one RStoic reactor was placed upstream of the methanation plant, to catalytically combust any O_2 in the flue gas using H_2 (O_2 is combined with H_2 to produce H_2O via catalysis rather than combustion) [33]. This additional stage is needed because O_2 deactivates the methanation catalyst. This is especially relevant for these decarbonisation concepts, since the flue gas contains around 3 - 9vol% O_2. Therefore, the H_2 required for these concepts was slightly higher than expected from the stoichiometry of Eq. (14), to account for the O_2.

3.4. *Methodology for the economic analysis*

The economic analysis considered capital expenditure (CAPEX), operational expenditure (OPEX) and income for the new and retrofitted

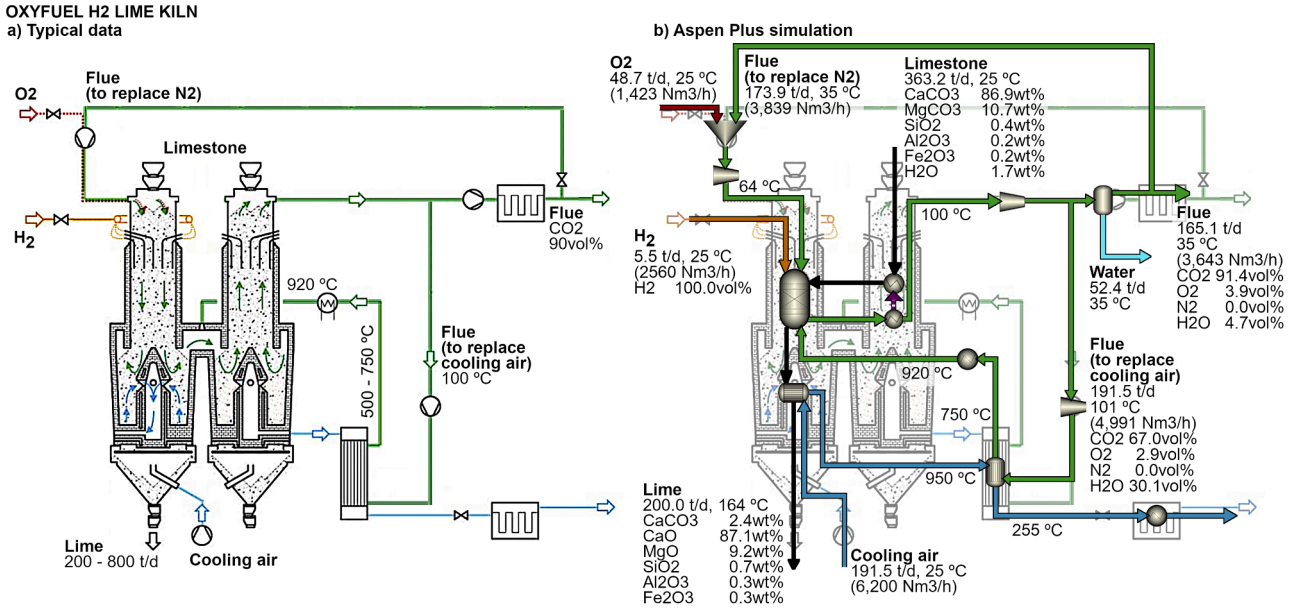

Fig. 7. Conceptual diagram (left) and Aspen Plus simulation (right) of an oxyfuel parallel flow regenerative H_2 lime kiln.

Table 3
Data for the economic analysis.

	Cost equation (M€) or (M€/year)	Parameters α, β, γ	Ref.
CAPEX			
Amine Plant	$43.49\cdot(\alpha/408)^{0.65}$	CO_2 captured [t/h]	[36, 37]
Electrolysis	$1750\cdot10^{-6}\cdot\alpha$	Power [kW]	[38]
H_2 storage			
H_2 storage tank	$563\cdot10^{-6}\cdot\alpha$	H_2 mass [kg_{H2}]	[39]
H_2 compressor	$0.267\cdot(\alpha/445)^{0.67}$	Power [kW]	[40]
Methanation			
CO_2 compressor	$0.267\cdot(\alpha/445)^{0.67}$	Power [kW]	[40]
Reactors	$300\cdot10^{-6}\cdot\alpha$	SNG power [kW_{SNG}]	[41]
Catalyst	$0.1875\cdot\alpha$	Volume of catalyst [m^3]	[40]
Lime kiln			
New lime kiln	$10^{-6}\cdot\alpha\cdot\beta$	New lime kiln price [€]	[42]
Solar			
PV plant	$750\cdot10^{-6}\cdot\alpha$	Power [kW]	-
Batteries	$500\cdot10^{-6}\cdot\alpha$	Battery size [kWh]	[43]
Thermal-solar field	$2344\cdot10^{-6}\cdot\alpha$	Solar field [kW]	[44]
Other direct costs			
Installation	$39\%\cdot\alpha$	Total equipment costs [€]	[45]
Instrumentation & control	$26\%\cdot\alpha$	Total equipment costs [€]	[45]
Piping	$31\%\cdot\alpha$	Total equipment costs [€]	[45]
Electrical	$10\%\cdot\alpha$	Total equipment costs [€]	[45]
Building	$29\%\cdot\alpha$	Total equipment costs [€]	[45]
Indirect costs			
Engineering	$32\%\cdot\alpha$	Total equipment costs [€]	[45]
Legal expenses	$4\%\cdot\alpha$	Total equipment costs [€]	[45]
Construction expenses	$34\%\cdot\alpha$	Total equipment costs [€]	[45]
Contingency	$37\%\cdot\alpha$	Total equipment costs [€]	[45]
OPEX			
Amine renovation	$3204\cdot10^{-6}\cdot\alpha$	MDEA renovation [tCO_2/year]	[46]
Catalyst renovation	$15\%\cdot\alpha$	Initial catalyst cost [M€]	[35]
Electricity	$10^{-6}\cdot\alpha\cdot\beta$	Electricity cost [€/MWh], Electricity purchased [MWh/year]	-
Water	$1.47\cdot10^{-6}\cdot\alpha$	Water consumption [m^3/year]	[47]
O&M	$3\%\cdot\alpha$	Total CAPEX	[36]
INCOMES			
Sold synthetic natural gas	$40\cdot10^{-6}\cdot\alpha$	SNG sold [MWh/year]	[48]
Saved fossil natural gas	$40\cdot10^{-6}\cdot\alpha$	NG saved [MWh/year]	[48]
Oxygen	$80\cdot10^{-6}\cdot\alpha$	O_2 generated [t_{O2}/year]	[49]
CO_2 taxes	$84.28\cdot10^{-6}\cdot\alpha$	CO_2 consumed [t_{CO2}/year]	[50]

components (Table 3). The CAPEX comprised the electrolyser, the methanation plant, the amine scrubbing/new lime kiln (depending on the decarbonisation pathway), the H_2 storage tank, as well as other direct and indirect costs. According to the IEAGHG [34], a new lime kiln cost approximately 19.8 M€ (inflation-adjusted). The OPEX included the catalyst renovation for methanation, the amine renovation, purchased electricity (77 €/MWh), required water, and operation and maintenance. The incomes were the savings in fossil natural gas (40 €/MWh), the synthetic natural gas sold (whenever surplus is found), the CO_2 taxes (84 €/t_{CO2}), and the oxygen sold. The loan amortisation was set at 20 years, with 8,000 hours of operation per year [35]. The specific carbon capture costs, expressed in €/t_{CO2} and €/t_{CaO}, were described in Eqs. (24) and (25), respectively.

$$\text{Specific Carbon Avoidance Cost} = \frac{\left(\frac{\text{CAPEX}}{\text{Loan amortisation}} + \text{OPEX} - \text{Incomes}\right)10^6}{\text{CO}_2\text{ avoided} \times \text{Operating hours}} \left[\frac{€}{t_{CO_2}}\right] \quad (24)$$

Table 4
Location and technical data of the PV solar field.

	Roof type 1	Roof type 1&2
PV panels		
Roof area (m^2)	141,048	704,101
Solar area (m^2)	98,734	380,621
Average system loss* (%)	35.6	35.6
Peak power (MWp)	14.8	56.8
Max. power production (MW)	11.5	44.1
Electricity production (MWh/year)	15,014	57,532
Equivalent operating hours (h)	1,013	1,013
Li-ion battery		
Round-trip efficiency (%)	85.0	85.0
Power capacity (MW)	0.74	2.84
Energy capacity (in time) (h)	4	4
Electricity processed (MWh/year)	603	2,405
Electricity provided (MWh/year)	512	2,044
Average charge (%)	9.5	10.1
Electrolyser		
Consumption (kWh/Nm^3)	4.50	4.50
Power capacity (MW)	6.9	25.6
Nominal H_2 production (Nm^3/h)	1,533	5,693
Nominal O_2 production (Nm^3/h)	766	2,846
Usage of PV electricity (%)	92.5	91.3
Electricity processed (MWh/year)	13,893	52,524
H_2 production (Nm^3/year)	3,087,288	11,671,965
O_2 production (Nm^3/year)	1,543,644	5,835,983
Equivalent operating hours (h)	2,014	2,050
Average capacity factor (%)	23.0	23.4
Average H_2 production (Nm^3/h)	352	1,332

* Including effects related to the angle of incidence and temperature

$$\text{Specific Implementation Cost} = \frac{\left(\frac{\text{CAPEX}}{\text{Loan amortisation}} + \text{OPEX} - \text{Incomes}\right)10^6}{\text{Lime production} \times \text{Operating hours}} \left[\frac{€}{t_{CaO}}\right] \quad (25)$$

4. Results and discussion

4.1. Renewable electricity and H_2 production

Following the methodology described above, the PV field was sized based on the available roof area. Then, the electrolyser was sized as a function of the load duration curve. Therefore, the results regarding the electricity and H_2 production were independent of the decarbonisation pathway selected for the lime kiln (only the size of the methanation plant had to be adjusted for each case). The Table 4 gathers the two PV scenarios analysed: (i) utilisation of the roof type 1, and (ii) utilisation of both the roof type 1&2. Type 3 roof was not considered due to the high investment required.

In PV systems, the ratio of solar area (usable area for power production) to available area (roof area) is typically 50-90%, depending on roof angle and surrounding shadows [51]. In our study, we assumed 70% for Type 1 and 50% for Type 2 (conservative approach). The total solar area for buildings ready for PV installation (i.e., Type 1) was 0.1 km^2, equivalent to 15 MWp of PV capacity. When considering the roofs that required moderate rehabilitation or cleaning (i.e., Type 2), the total solar area increased to 0.38 km^2, corresponding to 57 MWp of PV capacity. The auxiliary Li-ion batteries installed had round-trip energy storage capacities of 2.5 MWh (4 h × 0.74 MW × 0.85) and 9.7 MWh (4 h × 2.84 MW × 0.85), respectively.

The size of the electrolyser was chosen in order to maximise the energy that can be stored at nominal load, W_e^* (Fig. 8, left). Additionally, the criterion 2 described in Section 3.2 had to be applied, since there was a wide range of electrolyser sizes in which W_e^* was similar (e.g., for the roof Type 1&2, the value of W_e^* only varied ±1% for sizes between 19.8 MW and 25.6 MW, what can be observed in the flat-topped hill of the curve in Fig. 8, left). Hence, the selected electrolyser capacity was 6.9

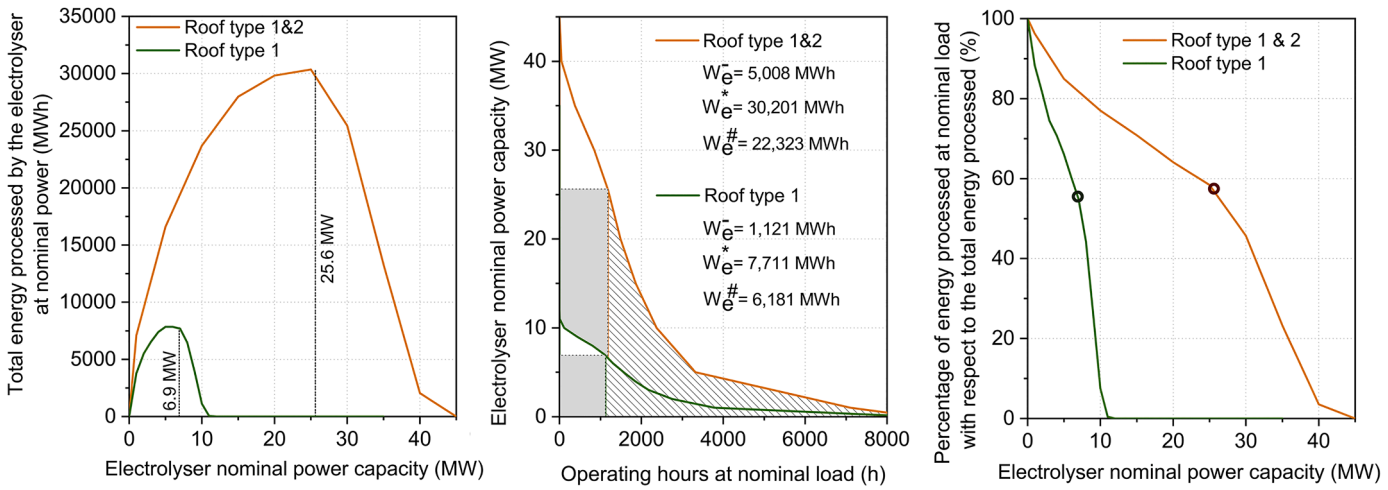

Fig. 8. Sizing of the electrolyser (6.9 MW for roof type 1, and 25.6 MW for roof type 1&2). Left: Total energy processed by the electrolyser at nominal power vs Electrolyser nominal power; Centre: Electrolyser nominal power vs Operating hours at nominal load (load duration curve); Right: Percentage of energy processed at nominal load with respect to the total energy processed vs Electrolyser nominal power.

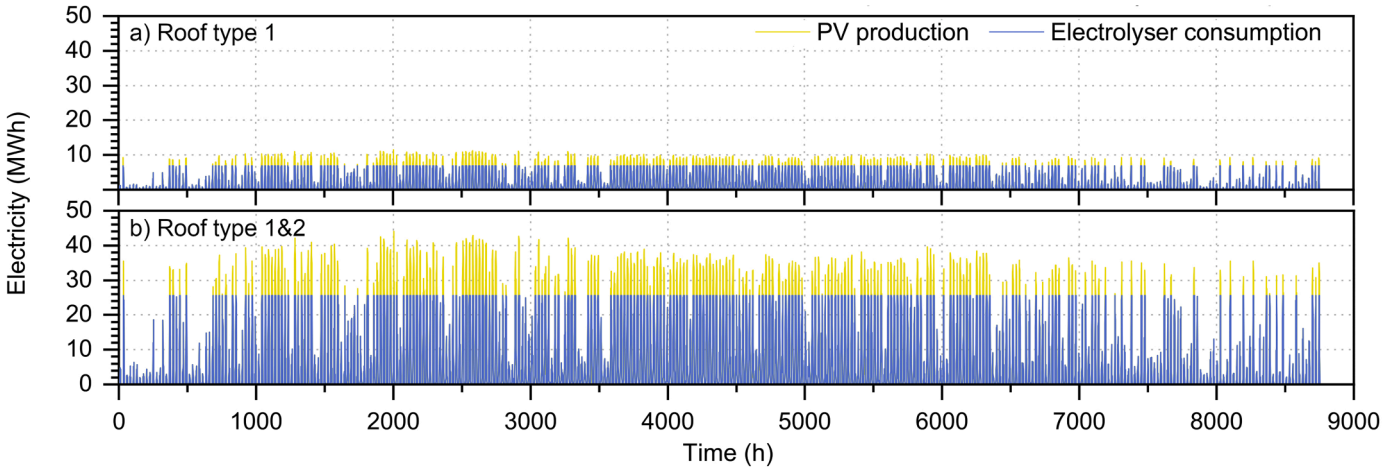

Fig. 9. PV electricity production (MWh) and Electrolysis electricity consumption (MWh) vs. time (h).

MW for the roof type 1 and 25.6 MW for the roof type 1&2. These solutions were depicted in the load duration curves of Fig. 8 (centre). The percentage of energy processed at nominal load relative to the total energy processed by the electrolyser, was between 55% and 57%. This point corresponds to a clear change in the slope of the curve of Fig. 8 (right), beyond which the percentage of energy stored at nominal load decreases faster (before this point, the percentage decreases just because the patter area of the LDC increases, while beyond this point the percentage decreases faster because the grey area starts getting smaller).

With this installation size, the yearly electricity production of the PV field was 15.0 GWh for the roof type 1, and 57.5 GWh for the combination of roof type 1&2, both with 1013 equivalent operating hours (Table 4). The 91-92% of this electricity could be used in the electrolyser, see Fig. 9 (the rest corresponds to the blank area under the LDC in Fig. 8, which should be discarded or used in other parts of the iron-making plant). Throughout the year, the Li-ion battery processed 0.6 GWh and 2.4 GWh, respectively, resulting in the recovery of 0.5 GWh and 2.0 GWh of electricity after accounting for losses (yearly-average charge of 10%). Therefore, the Li-ion battery was not only useful to palliate cloud-coverage, but also for transferring some part of the sun production from the noon to the evening (if the Li-ion battery were not present, only the 87.6% of the PV electricity could have been used in the electrolyser, instead of the 91-92%). The yearly H_2 production was 3.1 and 11.7 million Nm^3, for the roof type 1 and the roof type 1&2 scenarios, respectively. The electrolysis capacity factor was 23% (2014-2050 equivalent operating hours).

4.2. *CO_2 emissions and synthetic natural gas production*

As shown in the previous section, the H_2 available for a given PV scenario was the same across all decarbonisation options, as it depended only on the installed PV capacity. Consequently, the methanation plant sizing, in terms of H_2 consumption, was the same for all decarbonisation options. As described in the methodology section, the smaller the methanation plant, the larger the H_2 tank needed to match the electrolyser's production with the methanation demand. However, small methanation sizes allowed higher capacity factors, which are desirable for steady operations. Therefore, we minimised the methanation plant size constrained by a maximum reasonable H_2 tank size of 66,740 Nm^3. Thus, for Roof type 1, the nominal H_2 consumption of the methanation plant was 495 Nm^3/h (1.5 MW_{H2}), and for Roof type 1&2 the nominal H_2 consumption was 2,140 Nm^3/h (6.4 MW_{H2}). The equivalent operating hours were 6,238 h in the first case (71.2% capacity factor), and 5,454 h in the second case (62.3% capacity factor) (Fig. 10). Since the H_2 tank size was the same in both scenarios (Fig. 11), its contribution to maintaining high capacity factors in methanation are less significant as

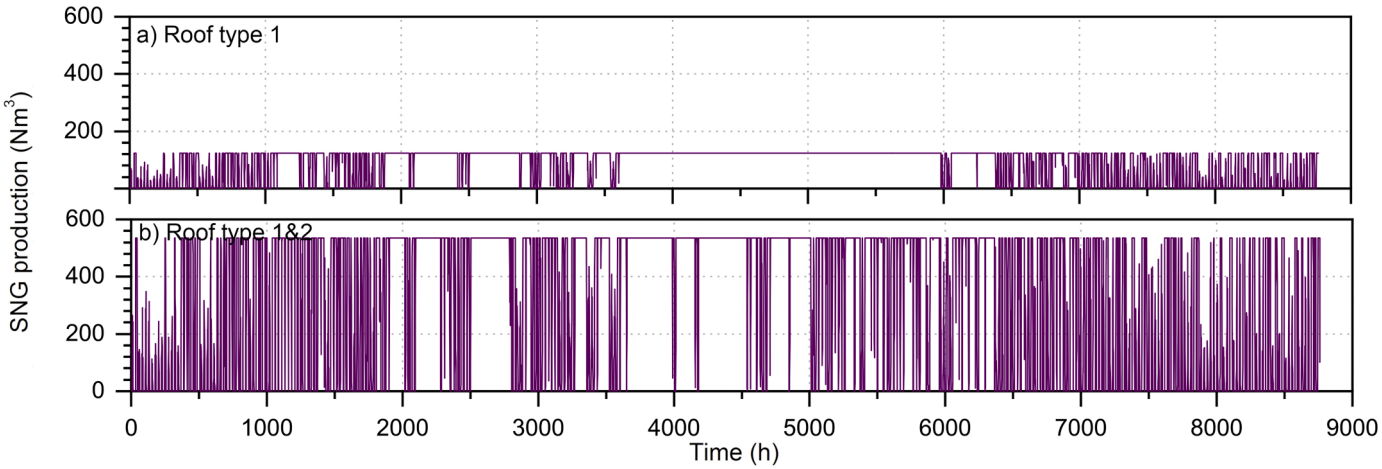

Fig. 10. Synthetic natural gas produced (Nm^3) vs. time (h).

PV power increases. The methanation plant's efficiency was always around 82–83%. The synthetic natural gas produced differed slightly due to small differences in the flue gas composition entering the methanation process for each concept. In particular, this dependency was considered for through the parameters $\epsilon_{m,i}$ (gas conversion efficiency) and $\nu_{m,i}$ (stoichiometry of methanation) appearing in Eqs. (22) and (23).

Regarding CO_2 emissions, the intrinsic characteristics of each concept led to different emission reductions (Table 5), as we had the option of providing heat for calcination with synthetic methane or H_2. Regarding the first PV scenario, in which only Roof type 1 was considered (Table 6), CO_2 emissions reductions were either 2% or 22% with respect to a conventional air-blown lime kiln with no mitigation measures. This difference mainly came from the strategy followed: the reduction was 2% if we partially replaced fossil natural gas by using the synthetic methane that was produced (carbon recycling), while the reduction was 22% if we avoided the fossil natural gas by directly using H_2 (and selling the synthetic methane produced).

In the first case, we had the option of either amine scrubbing or oxy-fuel combustion to capture CO_2 from the combustion. If we used amines, the energy penalty was 33.1 MJ/kg_{CO2}, which was due to electrolysis consumption. If we used oxy-fuel combustion, the energy penalty was 51.1 MJ/kg_{CO2}. The higher penalisation of the latter arose from the necessity of producing pure O_2 with an air separation unit (380 kWh/t_{O2} [52]), as the electrolyser could only provide the 10% of the O_2 required in the kiln. In both cases, the natural gas used in the lime kiln was around

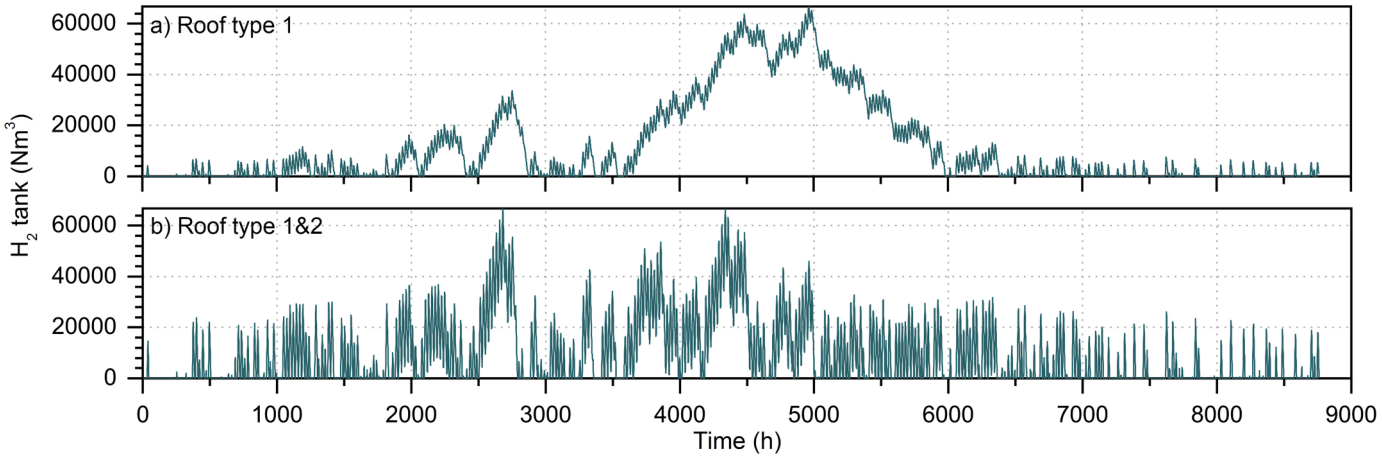

Fig. 11. H_2 stored in the tank (Nm^3) vs. time (h).

Table 5
CO_2 emissions, electricity consumption and specific energy penalty for the different decarbonisation pathways proposed. Minimum and maximum values depend on the total roof area for PV installation (corresponding to Roof type 1 and Roof type 1&2 areas, respectively).

Lime kiln technology	Air-blown	Air-blown + amines	Oxy-fuel	H_2 Oxy-fuel
CO_2 emissions (t_{CO2}/year)	68,000	66,855 – 62,657	66,877 – 62,741	53,521 – 49,394
CO_2 reduction (t_{CO2}/year)	-	1,510 – 5,707	1,488 – 5,624	14,844 – 18,971
CO_2 reduction (%)	-	2.2 – 8.3	2.2 – 8.2	21.7 – 27.7
Electricity consumption (TJ/year)				
Electrolyser (H_2 for methanation)	-	50.0 – 189.1	50.0 – 189.1	50.0 – 189.1
Electrolyser (H_2 for lime kiln)	-	-	-	348.8
ASU (O_2 for lime kiln)	-	-	26.0 – 11.4	0.0
Total	-	50.0 – 189.1	76.0 – 200.5	398.8 – 537.9
Energy penalty (MJ/kg_{CO2})	-	33.1	51.1 – 35.6	26.9 – 28.3

Table 6
Technical data assessment for the different decarbonisation pathways proposed, using the roof area of Roof type 1 for PV installation.

Decarbonisation pathway	Air-blow + amines	Oxy-fuel	H_2 Oxy-fuel
Lime kiln			
Nominal production (t_{Lime}/h)	8.3	8.3	8.3
Equivalent operating hours (h)	8410	8410	8410
Average capacity factor (%)	96.0	96.0	96.0
Yearly production (t_{Lime}/year)	70,083	70,083	70,083
Natural gas yearly consumption (Nm^3/year)	6,659,038	6,659,038	-
From Power to Gas (%)	11.7	11.6	-
From gas grid (%)	88.3	88.4	-
H_2 yearly consumption (Nm^3/year)	-	-	21,529,600
O_2 yearly consumption (Nm^3/year)	-	14,825,232	11,967,430
Flue gas yearly production (Nm^3/year)	169,491,776	37,962,908	30,637,630
CO_2 yearly production (t_{CO2}/year)	68,365	68,350	55,005
Recycled through Power to Gas (%)	2.2	2.2	2.7
Released to the atmosphere (%)	97.8	97.8	97.3
Electrolyser (sized for PV panels)			
Equivalent operating hours using PV (h)	2,014	2,014	2,014
Additional equivalent operating hours using grid to feed lime kiln (h)	-	-	6,386
Total equivalent operating hours (h)	2,014	2,014	8,400
Yearly H_2 production using PV (Nm^3/year)	3,087,288	3,087,288	3,087,288
Additional yearly H_2 production using grid (Nm^3/year)	-	-	9,789,186
Total yearly H_2 production (Nm^3/year)	3,087,288	3,087,288	12,876,474
Additional electrolyser (required to fulfil lime kiln needs)			
Power capacity (MW)	-	-	6.3
Equivalent operating hours (h)	-	-	8,400
Yearly H_2 production (Nm^3/year)	-	-	11,740,414
Methanation			
Conversion efficiency, ϵ (Nm^3_{SNG}/Nm^3_{H2})	0.2534	0.2498	0.2491
Stoichiometry, ν (mol_{H2}/mol_{CO2})	4.0170	4.0766	4.0856
Nominal H_2 consumption (Nm^3/h)	495	495	495
Nominal SNG production (Nm^3/h)	125.4	123.6	123.3
Equivalent operating hours (h)	6,238	6,238	6,238
Average capacity factor (%)	71.2	71.2	71.2
Yearly SNG production (Nm^3/year)	782,068	771,016	768,856
Diverted to lime kiln (%)	100.0	100.0	0.0
Sold to the gas grid (%)	0.0	0.0	100.0
LHV_{SNG} (MJ/Nm^3)	35.1	35.1	35.1
LHV_{SNG} (MJ/kg)	49.5	49.5	49.6
Molar mass SNG (kg/kmol)	15.87	15.88	15.87
Efficiency LHV (%)	82.9	81.8	83.4
H_2 tank			
Maximum capacity (Nm^3)	66,740	66,740	66,740
Yearly average capacity (%)	17.7	17.7	17.7
Other			
Amine scrubbing plant size (t_{CO2}/h)	0.24	-	-
O_2 production (Nm^3/year)	1,543,644	14,825,232	12,308,443
From ASU (%)	0.0	89.6	0.0
From Electrolyser (%)	100.0	10.4	12.5 + 39.8 + 47.7
O_2 for selling (Nm^3/year)	1,543,644	0	341,013

Table 7
Technical data assessment for the different decarbonisation pathways proposed, using the roof area of Roof type 1&2 for PV installation.

Decarbonisation pathway	Air-blow + amines	Oxy-fuel	H_2 Oxy-fuel
Lime kiln			
Nominal production (t_{Lime}/h)	8.3	8.3	8.3
Equivalent operating hours (h)	8410	8410	8410
Average capacity factor (%)	96	96.0	96.0
Yearly production (t_{Lime}/year)	70,083	70,083	70,083
Natural gas yearly consumption (Nm^3/year)	6,659,038	6,659,038	-
From Power to Gas (%)	43.7	43.8	-
From gas grid (%)	56.3	56.2	-
H_2 yearly consumption (Nm^3/year)	-	-	21,529,600
O_2 yearly consumption (Nm^3/year)	-	14,825,232	11,967,430
Flue gas yearly production (Nm^3/year)	169,491,776	37,962,908	30,637,630
CO_2 yearly production (t_{CO2}/year)	68,365	68,350	55,005
Recycled through Power to Gas (%)	8.4	8.2	10.2
Released to the atmosphere (%)	91.6	91.8	89.8
Electrolyser (sized for PV panels)			
Equivalent operating hours using PV (h)	2,050	2,050	2,050
Additional equivalent operating hours using grid to feed lime kiln (h)	-	-	3,782
Total equivalent operating hours (h)	2,050	2,050	5,832
Yearly H_2 production using PV (Nm^3/year)	11,670,650	11,670,650	11,670,650
Additional yearly H_2 production using grid (Nm^3/year)	-	-	21,529,600

(*continued on next page*)

Table 7 (*continued*)

Decarbonisation pathway	Air-blow + amines	Oxy-fuel	H_2 Oxy-fuel
Total yearly H_2 production (Nm^3/year)	11,670,650	11,670,650	33,200,250
Additional electrolyser (required to fulfill lime kiln needs)			
Power capacity (MW)	-	-	-
Equivalent operating hours (h)	-	-	-
Yearly H_2 production (Nm^3/year)	-	-	-
Methanation			
Conversion efficiency, ϵ (Nm^3_{SNG}/Nm^3_{H2})	0.2534	0.2498	0.2491
Stoichiometry, ν (mol_{H2}/mol_{CO2})	4.0170	4.0766	4.0856
Nominal H_2 consumption (Nm^3/h)	2,140	2,140	2,140
Nominal SNG production (Nm^3/h)	542	535	533
Equivalent operating hours (h)	5,454	5,454	5,454
Average capacity factor (%)	62.3	62.3	62.3
Yearly SNG production (Nm^3/year)	2,957,451	2,915,657	2,907,487
Diverted to lime kiln (%)	100.0	100.0	0.0
Sold to the gas grid (%)	0.0	0.0	100.0
LHV_{SNG} (MJ/Nm^3)	35.1	35.1	35.1
LHV_{SNG} (MJ/kg)	49.5	49.5	49.6
Molar mass SNG (kg/kmol)	15.87	15.88	15.87
Efficiency LHV (%)	82.9	81.8	83.4
H_2 tank			
Maximum capacity (Nm^3)	66,740	66.740	66.740
Yearly average capacity (%)	13.7	13.7	13.7
Other			
Amine scrubbing plant size (t_{CO2}/h)	1.1	-	-
O_2 production (Nm^3/year)	5,835,982	14,825,232	16,600,125
From ASU (%)	0.0	60.6	0.0
From Electrolyser (%)	100.0	39.4	35.2 + 64.8 + 0.0
O_2 for selling (Nm^3/year)	5,835,982	0	4,632,695

88% fossil and 12% renewable.

In the second strategy (22% CO_2 reduction) we used H_2 instead of fossil natural gas to provide the heat for calcination. This already provides a 20% reduction in CO_2 emissions compared to conventional operation, just from the total avoidance of the fossil fuels. The final emission reduction increases to 22% due to the production of synthetic methane with part of the flue gas.

Using H_2 as fuel, we needed to consume an additional 97 GWh/year of electricity to produce that hydrogen through electrolysis. Considering that the electrolysis capacity was 6.9 MW in this scenario, using our electrolyser to produce the additional H_2 resulted in increasing the electrolyser's operating hours from 2,014 to 16,057, which exceeds the annual period. Therefore, the H_2 lime kiln concept, under the Roof type 1 scenario, would require increasing electrolysis capacity to produce all the H_2 needed to replace the fossil natural gas, with the corresponding increase in investment. Assuming a maximum of 8400 operating hours (96% capacity factor), the total electrolyser capacity would be 13.2 MW, rather than 6.9 MW. This additional operation would use grid electricity from renewable sources, ensuring that no further emissions are associated with this concept.

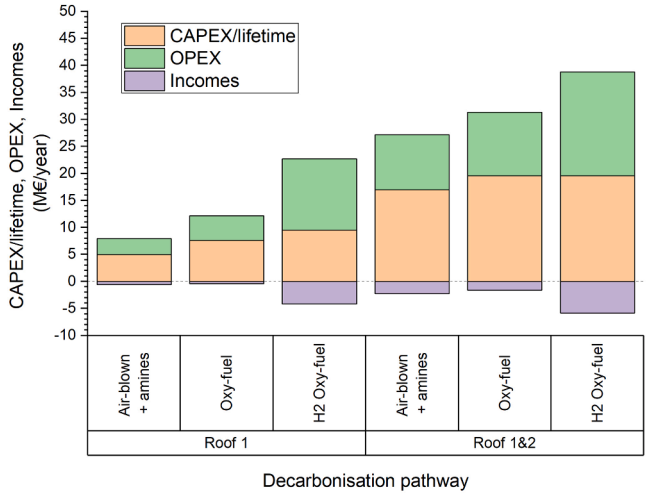

Fig. 12. Specific CAPEX (CAPEX/lifetime), OPEX and Incomes (M€/year), as a function of the decarbonisation pathway and the roof type.

The energy penalty of the H_2 lime kiln, under the first scenario, was 26.9 MJ/kg_{CO2}. Because of the high H_2 production in this case, there is an excess of O_2 available for sale (487 t_{O2}/year). The total O_2 is obtained as a byproduct from the electrolyser, 12.5% originated from the PV electricity, 39.8% from the grid electricity when increasing the operating hours to 8400 h in the initial electrolyser (6.9 MW), and 47.7% from the grid electricity associated with the additional electrolysis capacity required (6.3 MW).

Regarding the second scenario, in which the Roof types 1&2 were considered (Table 7), the qualitative results were similar. Given the higher installed PV capacity, the CO_2 emission reduction was between 8% and 28%. Only one important difference must be highlighted: the H_2 lime kiln did not require an additional increase in the installed electrolysis capacity (25.6 MW), since 5,832 operating hours were sufficient to produce the H_2 for both the calcination and the methanation processes.

4.3. Cash flow and specific costs

CAPEX, OPEX, and Income vary greatly depending on the decarbonisation pathway and the roof type selected (Fig. 12). The CAPEX for the different pathways ranges from 99 M€ for air-blown + amines and roof type 1 to 391 M€ for both Oxy-fuel and H_2 Oxy-fuel, and roof type 1&2 (Table 8). In all cases, the electrolyser represents the largest CAPEX share, followed by the PV plant. The cases with roof type 1&2 have larger PV plants, which led to larger electrolyser sizes and therefore higher CAPEX. The amines cost is only considered in the air-blown + amines case, but it is relatively low, especially compared to the electrolyser cost. Methanation costs remain consistent across the three scenarios, with a notably lower magnitude compared than the electrolyser cost.

The OPEX varies from 3.0 M€/year for air-blown + amines and roof type 1 to 19.2 M€/year for H_2 Oxy-fuel and roof type 1&2, see Fig. 12. For the latter pathway, the biggest OPEX share is the electricity, for both roof types 1 and 1&2, due to the large amount of hydrogen required.

Table 8
Results of the economic analysis of the decarbonisation routes for lime kilns in ironmaking plants.

Scenario	Type 1 Air-blown + amines	Type 1 Oxy-fuel	Type 1 H_2 Oxy-fuel	Type 1&2 Air-blown + amines	Type 1&2 Oxy-fuel	Type 1&2 H_2 Oxy-fuel
CAPEX [M€]	98.9	152.3	190.0	339.1	391.1	391.1
Amine Plant	0.35	0.00	0.00	0.56	0.00	0.00
Electrolysis	12.1	12.1	23.1	44.8	44.8	44.8
H_2 storage						
H_2 storage tank	3.38	3.38	3.38	3.38	3.38	3.38
H_2 compressor	0.120	0.120	0.120	0.120	0.281	0.281
Methanation						
CO_2 compressor	0.016	0.016	0.016	0.039	0.039	0.038
Reactors	0.367	0.362	0.361	1.585	1.565	1.559
Catalyst	0.005	0.005	0.005	0.022	0.022	0.022
Lime kiln						
New oxy lime kiln	0.0	16	16	0.0	16	16
Solar						
PV plant	11.10	11.10	11.10	42.60	42.60	42.60
Batteries	1.48	1.48	1.48	5.68	5.68	5.68
Other direct costs						
Installation	11.27	17.37	21.67	38.67	44.60	44.60
Instrumentation/ control	7.51	11.58	14.45	25.78	29.73	29.73
Piping	8.95	13.81	17.22	30.74	35.45	35.45
Electrical	2.89	4.45	5.56	9.92	11.44	11.44
Building	8.38	12.92	16.11	28.75	33.17	33.16
Indirect costs						
Engineering	9.24	14.25	17.78	31.73	36.60	36.59
Legal expenses	1.16	1.78	2.22	3.97	4.57	4.57
Construction expenses	9.82	15.14	18.89	33.71	38.88	38.88
Contingency	10.69	16.48	20.56	36.69	42.31	42.31
OPEX [M€/year]	2.97	4.57	13.18	10.19	11.75	19.21
Amine renovation	0.0006	0	0	0	0	0
Catalyst renovation	0.0008	0.0007	0.0007	0.0033	0.0032	0.0032
Electricity	0	0	7.47	0	0	7.46
Water	0.0041	0.0041	0.0078	0.0151	0.0151	0.0151
O&M	2.96	4.57	13.18	10.19	11.75	19.21
Incomes [M€/year]	0.61	0.43	4.19	2.29	1.61	5.85
Sold synthetic natural gas	0	0	0.30	0	0	1.13
Saved fossil natural gas	0.31	0.30	2.60	1.15	1.14	2.60
Oxygen	0.17	0	0.04	0.66	0	0.52
CO_2 taxes	0.13	0.13	1.25	0.48	0.47	1.60
Specific costs [€/t_{CO2}]	4836	7906	1246	4356	5280	1735
Specific costs [€/t_{CaO}]	110	176	277	373	445	494

Conversely, for the other pathways, the largest share is operation and maintenance (O&M). The Incomes ranges from 0.6 M€/y for oxy-fuel and roof type 1, to 5.9 M€/year for H_2 Oxy-fuel and roof type 1&2. In all cases, the main income is the natural gas (saved and sold) (Table 8). The income generated from the CO_2 taxes are significantly higher for the H_2 Oxy-fuel cases. This divergence can be attributed to the electrolyser's extended operating hours. However, OPEX is always higher than the Income.

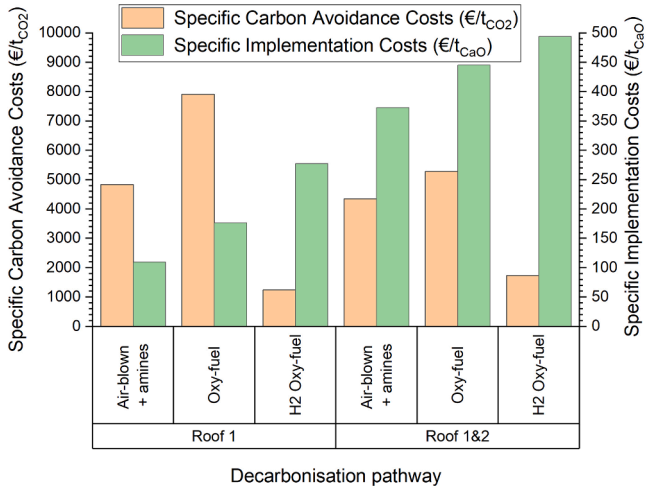

Fig. 13. Specific costs in €/t_{CO2} and €/t_{CaO}, as a function of the decarbonisation pathway and the roof type.

The specific carbon avoidance cost and the specific implementation cost, calculated with Eq. (24) and Eq. (25), are shown in Fig. 13. For roof type 1, the carbon avoidance cost is higher for Air-blown + amines and Oxy-fuel cases, owing to the lower operating hours of the electrolyser (2014 h), compared to the H_2 Oxy-fuel case (8400 h). For roof type 1&2, the same trend is observed, with higher costs for the two former cases (with 2050 h operating hours of the electrolyser), and lower costs for the latter case (with 5832 h). The implementation costs are directly related to the PV plant and electrolyser sizes, being higher in cases with roof type 1&2. Consequently, it is reasonable to assert that maximising the operating hours of the PtG system's electrolyser is recommended for optimal performance. Based on the results, H_2 Oxy-fuel is the best decarbonisation pathway for both roof type 1 and 1&2.

Implementing this technology after the current lime kiln's lifetime presents an opportunity to build a new one that meets new requirements, such as oxy-combustion with natural gas or with H_2. Amortising the cost of the new lime kiln against the lime produced could reduce specific costs. Specifically, the oxy-fuel and H_2 oxy-fuel cases with roof types 1 and 1&2 pathways can reduce specific costs by 7% to 19%.

5. Conclusions

The iron and steel industry requires diverse decarbonisation strategies. Challenges remain in achieving complete decarbonisation, especially in essential processes like lime kilns. To address these challenges, innovative pathways utilising Power to Gas technology have been explored. By establishing carbon recycling concepts, these pathways aim to effectively reduce CO_2 emissions. The analysis includes various technologies: (1) conventional lime kiln integrated with amine scrubbing, (2) Oxy-fuel lime kiln, and (3) Oxy-fuel H_2 lime kiln. The integration of Power to Gas is facilitated through solar power, with PV panels installed on the rooftops of a steelworks located in Austria.

This study employs simulation to evaluate the integration of Power to Gas across different lime kiln technologies. The renewable resource has been managed through a decision-making methodology based on an hourly basis. This methodology utilises the load operating curve to maximise the energy processed by each piece of equipment at full load. Furthermore, the various process diagrams have been simulated in Aspen Plus under steady-state operation. Then, it has been evaluated economically using a 'factored estimated' methodology, which is based on the knowledge of major items of equipment (this methodology has an accuracy of ±30%).

The available roof area was determined by classifying roofs by their suitability for PV panel installation. Type 1 roofs are ready for PV panel installation and are not significantly affected by surrounding conditions like shadows or dust. Type 2 roofs require rehabilitation and/or moderate measures to mitigate ambient dust for PV panel installation, necessitating additional investment. Type 1 roofs alone accounted for 0.1 km^2, equivalent to 15 MWp of PV capacity. Considering Type 2 roofs the total solar area increased to 0.38 km^2, corresponding to 57 MWp of PV capacity. The selected electrolyser capacities were 6.9 MW for Type 1 roofs and 25.6 MW for Type 1&2 roofs. With these installation sizes, the annual electricity production for Type 1 roofs was 15.0 GWh, and for Type 1&2 roofs, it was 57.5 GWh, both with 1,013 equivalent operating hours. Approximately 91-92% of this electricity could be utilised in the electrolyser. The annual H_2 production was 3.1 million Nm^3 for Type 1 roofs and 11.7 million Nm^3 for Type 1&2 roofs, with an electrolysis capacity factor of 23%.

The methanation plant size was optimised while adhering to a maximum reasonable H_2 tank size of 66,740 Nm^3. This resulted in a nominal hydrogen consumption of 495 Nm^3/h for Roof type 1 and 2,140 Nm^3/h for Roof types 1&2, with corresponding equivalent operating hours of 6,238 h (71.2% capacity factor) and 5,454 h (62.3% capacity factor), respectively. The methanation plant's efficiency consistently ranged between 82% and 83%.

In the first PV scenario involving only Roof type 1, CO_2 emissions reductions ranged from 2% to 22% compared to a conventional air-blown lime kiln with no mitigation measures. This variation depended on the strategy employed: a 2% reduction occurred when partially replacing fossil natural gas with synthetic methane, while a 22% reduction was achieved by directly using H_2 and selling the synthetic methane produced. Employing amine scrubbing or oxy-fuel combustion strategies for CO_2 capture resulted in energy penalties of 33.1 MJ/kg_{CO2} and 51.1 MJ/kg_{CO2}, respectively. The energy penalty of the H_2 lime kiln under the first scenario was 26.9 MJ/kg_{CO2}. In the second scenario involving Roof types 1&2, CO_2 emissions were reduced by 8% to 28%, with conclusions similar to those in the first scenario.

Regarding the economic analysis, CAPEX ranges from 99 M€ to 391 M€, with the electrolyser representing the largest share. OPEX ranges from 3.0 M€/year to 19.2 M€/year, with electricity accounting for the largest share only for H_2 Oxy-fuel. Incomes range from 0.6 M€/year to 5.9 M€/year, mainly from natural gas savings. Carbon avoidance costs are higher for Air-blown + amines and Oxy-fuel due to lower electrolyser operating hours. Implementing H_2 Oxy-fuel is recommended against the other options, but all of them provide specific capture cost well beyond reasonable values (>1000 €/t_{CO2}). Therefore, the complete decarbonisation of the steel production chain remains a challenge, and it is far from achievable solely with H_2 and synthetic fuels.

CRediT authorship contribution statement

Manuel Bailera: Writing – original draft, Visualization, Validation, Software, Methodology, Investigation, Funding acquisition, Formal analysis, Conceptualization. **Alexander García-Mariaca:** Writing – original draft, Validation, Methodology. **Cristian Barón:** Writing – original draft, Visualization, Validation, Methodology.

Declaration of competing interest

The authors declare that they have no known competing financial interests or personal relationships that could have appeared to influence the work reported in this paper.

Acknowledgments

This project has received funding from the European Union's Framework Programme for Research and Innovation Horizon 2020 (2014-2020) under the Marie Skłodowska-Curie Grant Agreement No. 887077. This publication is supported by RYC2022-038283-I, funded by MCIN/AEI/10.13039/501100011033 and the European Social Fund Plus (FSE+). This article is part of the R&D project PID2023-149968OB-I00, funded by MICIU/AEI/10.13039/501100011033/ and by FEDER, UE. The FPU Programme of the Spanish Ministry of Science, Innovation and Universities (FPU/00073) provided financial support for Cristian Barón PhD studies. Aspen Technology Inc is also acknowledged for the use of the software. MB acknowledges the employees of K1-MET and Voestalpine Linz for their discussions about the topic.

Supplementary materials

Supplementary material associated with this article can be found, in the online version, at doi:10.1016/j.rineng.2026.110076.

Data availability

No data was used for the research described in the article.

References

[1] H. Piringer, P. Bucher, R. Wallimann, Sustainable lime burning technology with shaft kilns, ZKG Cem. Lime Gypsum (2021).
[2] A. Cores, L.F. Verdeja, S. Ferreira, Í Ruiz-Bustinza, J. Mochón, J.I. Robla, et al., Iron ore sintering. Part 3: Automatic and control systems, Dyna (Medellin) 82 (2015) 227–236, https://doi.org/10.15446/dyna.v82n190.44054.
[3] Remus R, Aguado-Monsonet MA, Roudier S, Delgado L. Best available techniques (BAT) reference document for iron and steel production. 2013. doi:10.2791/98516.
[4] M. Bailera, Comparing different syngas for blast furnace ironmaking by using the extended operating line methodology, Fuel 333 (2023) 126533, https://doi.org/10.1016/j.fuel.2022.126533.
[5] F. Zhang, Y. Zhou, W. Sun, S. Hou, L. Yu, CO2 capture from reheating furnace based on the sensible heat of continuous casting slabs, Int. J. Energy Res. 42 (2018) 2273–2283, https://doi.org/10.1002/er.4020.
[6] Energy NL. REF BOF steelmaking – greenfield 2020. https://energy.nl/data/ref-bof-steelmaking-greenfield/(accessed February 1, 2024).
[7] J-W Moon, S-J Kim, Y. Sasaki, Effect of Preheated Top Gas and Air on Blast Furnace Top Gas Combustion, ISIJ Int. 54 (2014) 63–71, https://doi.org/10.2355/isijinternational.54.63.
[8] A. Cores, L.F. Verdeja, S. Ferreira, Í Ruiz-Bustinza, J. Mochón, J.I. Robla, et al., Iron ore sintering. Part 3: automatic and control systems, Dyna (Medellin) 82 (2015) 227–236, https://doi.org/10.15446/dyna.v82n190.44054.
[9] Remus R, Aguado-Monsonet MA, Roudier S, Delgado L. Best Available Techniques (BAT) reference document for iron and steel production. 2013. doi:10.2791/98516.
[10] F. Zhang, Y. Zhou, W. Sun, S. Hou, L. Yu, CO2 capture from reheating furnace based on the sensible heat of continuous casting slabs, Int. J. Energy Res. 42 (2018) 2273–2283, https://doi.org/10.1002/er.4020.

[11] M. Bailera, P. Lisbona, B. Peña, LM. Romeo, A review on CO2 mitigation in the Iron and Steel industry through Power to X processes, J. CO2 Util. 46 (2021) 101456, https://doi.org/10.1016/j.jcou.2021.101456.
[12] Vale makes pellets using renewable energy sources for the first time 2023.
[13] H. Sefidari, B. Lindblom, L-O Nordin, H. Wiinikka, The Feasibility of Replacing Coal with Biomass in Iron-Ore Pelletizing Plants with Respect to Melt-Induced Slagging, Energies 13 (2020) 5386, https://doi.org/10.3390/en132053861.
[14] RI. Birley, Decarbonising the DRI feed for EAF using H2, 12th Eur. Electr. Steelmak. Conf. (2021).
[15] T. Echterhof, Review on the Use of Alternative Carbon Sources in EAF Steelmaking, Metals 11 (2021) 222, https://doi.org/10.3390/met11020222.
[16] H. Piringer, P. Bucher, R. Wallimann, Sustainable lime burning technology with shaft kilns, ZKG Cem. Lime Gypsum (2021).
[17] European Commission. PVGIS ver. 5.2 2022.
[18] Center for Sustainable Systems University of Michigan. Photovoltaic energy factsheet 2021;CSS07-08.
[19] International Energy Agency. Special Report on Solar PV Global Supply Chains 2022.
[20] Google Maps, Satellite image for Voestalpine steelworks in Linz, Austria (48°16'38,2"N 14°19'58,7"E) (2022).
[21] Iberdrola. Puertollano: Green hydrogen plant for industrial use (Infographic) 2022.
[22] National Rural Utilities Cooperative Finance Corporation. Battery Energy Storage Overview 2019.
[23] M. Bailera, P. Lisbona, B. Peña, LM. Romeo, Energy Storage, Springer International Publishing, Cham, 2020, https://doi.org/10.1007/978-3-030-46527-8.
[24] M. Bailera, B. Peña, P. Lisbona, LM. Romeo, Decision-making methodology for managing photovoltaic surplus electricity through Power to Gas : Combined heat and power in urban buildings, Appl. Energy 228 (2018) 1032–1045, https://doi.org/10.1016/j.apenergy.2018.06.128.
[25] NEL Hydrogen. M Series Containerized Proton Exchange Membrane (PEM) Hydrogen Generation Systems 2021.
[26] MAERZ. The PFR Principle: How the PFR kiln works 2022. https://www.maerz.com/maerz-products/maerz-lime-kilns/the-pfr-principle#start (accessed November 4, 2022).
[27] Aspen Technology Inc. Aspen Physical Property Methods - Reference Manual 2019.
[28] F. Shi, Reactor and Process Design in Sustainable Energy Technology, Elsevier, 2014.
[29] Perpiñán J, Bailera M, Peña B, Romeo LM, Eveloy V. Technical and economic assessment of iron and steelmaking decarbonisation via power to gas and amine scrubbing 2022.
[30] MAERZ, MAERZ EcoKilns®: How does the Maerz EcoKiln® work?. https://www.maerz.com/maerz-products/maerz-lime-kilns/maerz-ecokilns/the-ecokilns-concept#start, 2022 (accessed November 4, 2022).
[31] Aspen Technology Inc. Aspen Physical Property Methods - Reference Manual 2019.
[32] K. Izumiya, I. Shimada, Methane producing technology from CO2 for carbon recycling, First Symp. Carbon Ultim. Util. Technol. Glob. Environ. CUUTE-1 (2021) 34–35.
[33] R. Jones, K. McIntush, C. Wallace, Oxygen removal in natural gas systems, Gas Process. Assoc. Res. Rep. RR No 073 (2010).
[34] IEAGHG. Iron and steel CCS study (techno-economics integrated steel mill), Report 2013/2014, July 2013. 2013.
[35] M. Bailera, S. Espatolero, P. Lisbona, LM. Romeo, Power to gas-electrochemical industry hybrid systems: a case study, Appl. Energy 202 (2017) 435–446, https://doi.org/10.1016/j.apenergy.2017.05.177.
[36] M.R.M. Abu-Zahra, J.P.M. Niederer, P.H.M. Feron, GF. Versteeg, CO2 capture from power plants. Part II. A parametric study of the economical performance based on mono-ethanolamine, Int. J. Greenh. Gas Control 1 (2007) 135–142, https://doi.org/10.1016/S1750-5836(07)00032-1.
[37] FRED Economic data. Producer Price Index by Industry: Chemical Manufacturing n.d.
[38] International Energy Agency. Global Hydrogen Review 2023. 2023. https://doi.org/10.1787/a15b8442-en.
[39] S.M. Ali, J. Andrews, Low-cost storage options for solar hydrogen systems for remote area power supply, in: 16th World Hydrogen Energy Conference 2006, WHEC 2006 2, 2006, pp. 1269–1279.
[40] M. De Saint Jean, P. Baurens, C. Bouallou, K. Couturier, Economic assessment of a power-to-substitute-natural-gas process including high-temperature steam electrolysis, Int. J. Hydrog. Energy 40 (2015) 6487–6500, https://doi.org/10.1016/j.ijhydene.2015.03.066.
[41] M. Lehner, R. Tichler, H. Steinmüller, M. Koppe, Power-to-Gas: Technology and Business Models, Springer International Publishing, Cham, 2014, https://doi.org/10.1007/978-3-319-03995-4.
[42] IEAGHG. Iron and steel CCS study (techno-economics integrated steel mill), Report 2013/2014, July 2013. 2013.
[43] Lazard. Lazard's Levelized Cost of Storage Analysis—Version 5.0. 2019.
[44] J. García-Ferrero, R.P. Merchán, M.J. Santos, A. Medina, A. Calvo Hernández, Brayton technology for Concentrated Solar Power plants: Comparative analysis of central tower plants and parabolic dish farms, Energy Convers. Manage. 271 (2022), https://doi.org/10.1016/j.enconman.2022.116312.
[45] M.S. Peters, K.D. Timmerhaus, RE. West, Plant Design and Economics for Chemical Engineers, 5th ed., McGraw-Hill, 2003.
[46] Kohl AL, Nielsen RB. Gas Purification. 1997. https://doi.org/10.1016/B978-0-88415-220-0.X5000-9.
[47] G. Benjaminsson, J. Benjaminsson, RB. Rudberg, Power-to-Gas - A technical review, Sven. Gastek. Cent. AB; (2013).
[48] MibGas 2026. https://www.mibgas.es/(accessed February 24, 2026).
[49] Hurskainen M. Industrial oxygen demand in Finland. VTT Technical Research Centre of Finland. VTT Research Report; No VTT-R-06563-17 2017.
[50] SENDECO2 2022.
[51] IASOL (Technical consultation) 2022.
[52] Perpiñán J, Bailera M, Peña B, Romeo LM, Eveloy V. Technical and economic assessment of iron and steelmaking decarbonisation via power to gas and amine scrubbing 2022.